



# CHORUS

This is the accepted manuscript made available via CHORUS. The article has been published as:

## Doping a bad metal: Origin of suppression of the metal-insulator transition in nonstoichiometric VO<sub>2</sub>

P. Ganesh, Frank Lechermann, Ilkka Kylänpää, Jaron T. Krogel, Paul R. C. Kent, and Olle Heinonen

Phys. Rev. B **101**, 155129 — Published 23 April 2020

DOI: [10.1103/PhysRevB.101.155129](https://doi.org/10.1103/PhysRevB.101.155129)

# Doping a Bad Metal: Origin of Suppression of Metal-Insulator Transition in Non-Stoichiometric VO<sub>2</sub>

P. Ganesh,<sup>1,\*</sup> Frank Lechermann,<sup>2</sup> Ilkka Kylänpää,<sup>3,4</sup> Jaron Krogel,<sup>3</sup> Paul R. C. Kent,<sup>1,5</sup> and Olle Heinonen<sup>6</sup>

<sup>1</sup>*Center for Nanophase Materials Sciences, Oak Ridge National Laboratory, Oak Ridge, Tennessee, 37831, USA*

<sup>2</sup>*I. Institut für Theoretische Physik, Universität Hamburg, Jungiusstr. 9, D-20355 Hamburg, Germany*

<sup>3</sup>*Material Science and Technology Division, Oak Ridge National Laboratory, Oak Ridge, Tennessee, 37831, USA*

<sup>4</sup>*Computational Physics Laboratory, Tampere University, P.O. Box 692, FI-33014 Tampere, Finland*

<sup>5</sup>*Computational Sciences and Engineering Division,*

*Oak Ridge National Laboratory, Oak Ridge, Tennessee, 37831, USA*

<sup>6</sup>*Materials Science Division, Argonne National Laboratory, Lemont, Illinois 60439, USA*

(Dated: March 20, 2020)

Rutile ( $R$ ) phase VO<sub>2</sub> is a quintessential example of a strongly correlated bad-metal, which undergoes a metal-insulator transition (MIT) concomitant with a structural transition to a V-V dimerized monoclinic ( $M_1$ ) phase below  $T_{MIT} \sim 340K$ . It has been experimentally shown that one can control this transition by doping VO<sub>2</sub>. In particular, doping with oxygen vacancies ( $V_O$ ) has been shown to completely suppress this MIT *without* any structural transition. We explain this suppression by elucidating the influence of oxygen-vacancies on the electronic-structure of the metallic  $R$  phase VO<sub>2</sub>, explicitly treating strong electron-electron correlations using dynamical mean-field theory (DMFT) as well as diffusion Monte Carlo (DMC) flavor of quantum Monte Carlo (QMC) techniques. DMC calculations show a gap-closure in the  $M_1$  phase when vacancies are present, suggesting that when vacancies are introduced in the high-temperature rutile phase, the dimerized insulating phase cannot be reached when temperature is lowered. Both DMFT and DMC calculations of non-stoichiometric metallic rutile-phase shows that this tendency not to dimerize in the presence of vacancies is because  $V_O$ 's tend to change the V-3d filling away from its nominal half-filled value, with the  $e_g^\pi$  orbitals competing with the otherwise dominant  $a_{1g}$  orbital. Loss of this near orbital polarization of the  $a_{1g}$  orbital is associated with a weakening of electron correlations, especially along the V-V dimerization direction. This removes a charge-density wave (CDW) instability along this direction above a critical doping concentration, which further suppresses the metal-insulator transition. Our study also suggests that the MIT is predominantly driven by a correlation-induced CDW instability along the V-V dimerization direction.

## I. INTRODUCTION

Defects determine and control properties of solids and to a large degree impart specific functionalities to them. [1] Harvesting these functionalities will play a key role in advanced electronic materials for future information technologies, such as neuromorphic [2] and quantum computing. [3] There is a significant gap in our understanding of how defects influence technologically relevant phase transitions, such as the metal-insulator transition (MIT), in strongly correlated materials [4, 5]. Closing this gap is particularly challenging when strong non-local electron-electron correlation effects are coupled with the strong local interactions of defects with the lattice [6–8]; such a fundamental understanding is necessary for paving the way for robust future technologies based on correlated materials.

VO<sub>2</sub> is formally a  $3d^1$  system which is expected to have a metallic ground-state owing to its half-filled  $d$ -band. While indeed metallic at high temperatures, the compound is in a “bad metal”-regime because its resistivity is above the Mott-Ioffe-Regel bound [9, 10]. Below the transition temperature –  $T_{MIT} \sim 340 K$ , VO<sub>2</sub> becomes insulating. [11, 12] This electronic transition is accompanied by a structural phase transition,

in which the high-temperature and high-symmetry rutile ( $R$ ) phase [Fig. 1(a)] transforms to a low-temperature low-symmetry monoclinic ( $M$ ) phase by the formation of V-V dimers along the rutile  $c$  axis. As such this MIT is considered a Peierls-Mott type transition. [13, 14]. It has been a long-standing problem to understand if the MIT is driven primarily by electron correlations [15] or by intrinsic structural instabilities [16], and understanding this is crucial to the control of MIT in correlated solids.

The nominally V<sup>4+</sup> vanadium atoms in the rutile phase sit at the center of distorted oxygen octahedra. This splits the otherwise low-energy triply degenerate  $t_{2g}$  manifold of V-3d into a single  $a_{1g}$  orbital and a doubly degenerate  $e_g^\pi$  combination of orbitals. It is the  $a_{1g}$  orbital in the rutile phase that takes part in forming the dimerized singlet state across the MIT, thereby opening up an electronic gap. Indeed, detailed x-ray absorption, x-ray diffraction and transport studies on thin films across the MIT reveal tunability of  $T_{MIT}$  through strain or inter-diffusion, which appears to correlate with changes in  $a_{1g}$  orbital occupancy. [15, 17, 18]

Doping VO<sub>2</sub> with external substitutional dopants such as W in the V site has been shown to tune  $T_{MIT}$ , and partially reverts transport back to normal behavior. [10] Doping thin films of metallic  $R$  phase VO<sub>2</sub> with intrinsic oxygen vacancies was recently shown to fully suppress

the metal to insulator transition with no observed structural transitions down to 50 K. [19] It is not clear what is the underlying mechanism behind the tunability or suppression of the MIT with doping, and how this tunability/suppression depends on the doping concentration or the type of dopant. Understanding this can perhaps also reveal what factors are crucial in driving the MIT in the first place in stoichiometric  $\text{VO}_2$ .

In this article, we investigate the influence of doping  $\text{VO}_2$  with  $V_O$  and both capture and explain the experimentally observed suppression of the Peierls-Mott type MIT. We accomplish this by using density functional theory based methods (DFT and DFT+U), together with correlated-electronic structure methods, such as dynamical mean-field theory (DMFT) [20] and quantum Monte Carlo (QMC) [21]. QMC is a very accurate ground state correlated-method which gives accurate vacancy formation energies and electron densities. The use of DMFT allows us to expand the investigation into excited state spectra. We obtain critical insights on what factors are crucial in driving and controlling the MIT in  $\text{VO}_2$ , which should be relevant for similar bad-metal systems. [22–24] We also assess the importance of including electronic correlations in describing the physics of doping with defects and elucidate the link between correlations and orbital

filling. We conclude that electronic interactions are the primary driver of the MIT, and the structural distortion is a secondary consequence.

## II. METHODS

We perform electronic-structure calculations using a series of complimentary methodologies, that allow us to capture effects of structural distortions, account for strong electron correlations on the V sites, and access both ground- and excited-state properties, with cross-validation of computed quantities whenever possible. The following subsections detail the different methodologies we have employed.

### a. Density Functional Theory (DFT)

Atomic structures were relaxed using atomic forces obtained from non-spin polarized Density Functional Theory (DFT) based calculations with the SCAN meta-generalized-gradient (meta-GGA) functional [25, 26] as well as the Perdew, Burke, and Ernzerhof (PBE) functional with a Hubbard ‘U’ i.e. PBE+U, with  $U=4\text{eV}$  in the rotationally invariant Dudarev [27] approach, as implemented in the VASP package [28] using PAW pseudopotentials [29]. All calculations were performed in a 48-atom supercell with dimensions:  $L_x = L_y = 6.4412 \text{ \AA}$  and  $L_z = 11.4112 \text{ \AA}$ , along the orthogonal  $\mathbf{a}, \mathbf{b}, \mathbf{c}$  directions as shown in Fig.1(a) in the main-text. Atomic relaxations were performed using a  $4 \times 4 \times 4$   $\mathbf{k}$ -mesh to perform the Brillouin-zone integration with a gaussian-smearing of 0.2 and a plane-wave kinetic-energy cutoff of 400 eV, using the ‘accurate’ setting for the precision tag in VASP. The ‘V’ and ‘O’ PAW potentials had 13 and 6 valence electrons, respectively. Forces were converged down to  $0.01 \text{ eV/\AA}$ . The supercell Oxygen vacancy structures were obtained by removing one oxygen-atom from the 48-atom supercell (corresponding to  $\text{VO}_{2-\delta}$  with  $\delta=0.0625$ ). The SCAN and PBE+U total density-of-states (DOS) for pure and non-stoichiometric  $\text{VO}_2$  are shown in the Appendix figures 8 and 9.

### b. Quantum Monte Carlo (QMC)

The Diffusion Monte Carlo (DMC) flavor of continuum quantum Monte Carlo methods was performed on the same structure using QMCPACK[30]. Diffusion Monte Carlo is a highly accurate wavefunction based projector method that improves variationally as the starting, or trial, wavefunction is improved. An accurate trial wavefunction is essential to minimize residual fixed node/phase error in the method. The basic form of the trial wavefunction used here is a product of an up/down

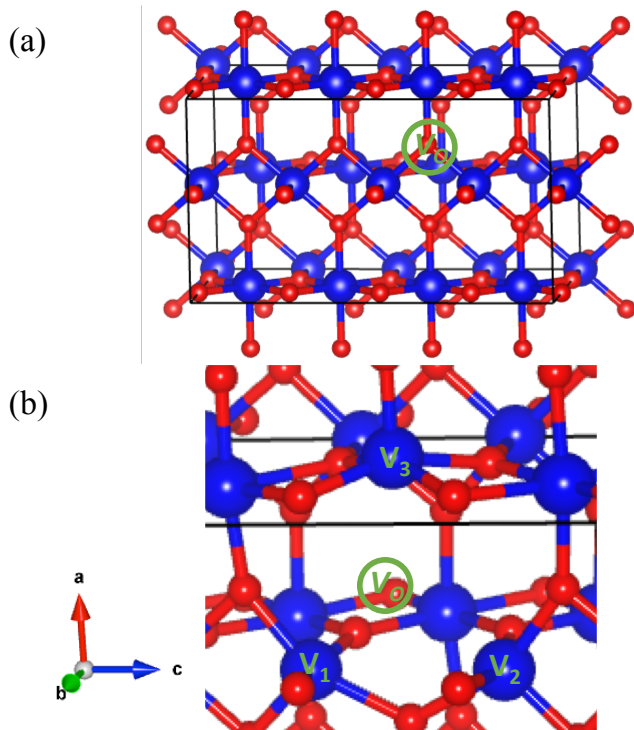


FIG. 1. (a) shows the DFT-SCAN relaxed structure of our 48-atom  $\text{VO}_2$  supercell. The  $V_O$  site is labeled. (b) shows the strong local distortions seen around the  $V_O$  site in relaxed  $\text{VO}_{2-\delta}$ . The nearest neighbor V-atoms to the  $V_O$  site are also labeled. (V(blue), O(red))

spin factorized Slater determinant and a Jastrow correlation factor, as follows:

$$\Psi_T(R) = e^{J(R)} D^\uparrow(R^\uparrow) D^\downarrow(R^\downarrow). \quad (1)$$

The nodal/phase structure of the trial wavefunction is determined by the single particle orbitals populating the determinants. Trial orbitals were obtained within LSDA+U via the Quantum Espresso code for all atomic structures. The U value was selected to be 3.5 eV since this value minimizes the variational DMC total energy for VO<sub>2</sub> as demonstrated by prior studies [6, 31]. A ferromagnetic configuration was chosen for the V-sites since this arrangement of magnetic moments is more robust to changes in the lattice induced by defects. Since the spin gap in the materials is small, this choice has a negligible impact on the resulting defect formation energies. The trial Jastrow factor was represented as a sum of one- and two-body correlation factors represented in a B-spline basis along electron-electron or electron-ion pair distances. The Jastrow factor was variationally optimized with re-

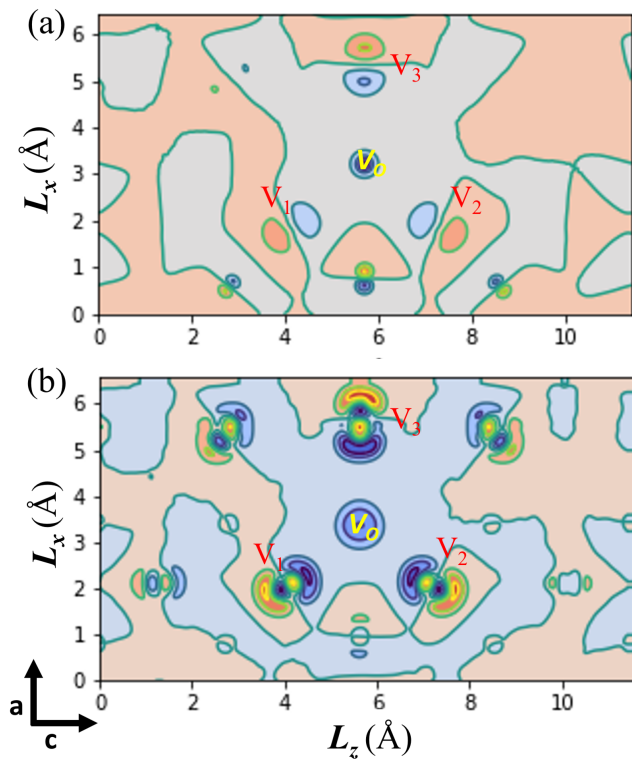


FIG. 2. Contour plots of charge-density difference (units of  $e/(a.u.)^3$ ) between non-stoichiometric and stoichiometric VO<sub>2</sub> in the central plane containing the  $V_O$  from (a) DMFT and (b) QMC calculations. Both levels of theory suggest that electronic reorganization propagates from local changes around the defect site. The three V-atoms closest to the  $V_O$  site [labeled in Fig. 1(b)], show the largest density changes. (blue/red show density loss/gain compared to pristine VO<sub>2</sub>). The color-bar ranges from  $\{-4, 3\}$  and  $\{-1.2, 1.2\}$  for DMFT and QMC plots, respectively.)

spect to the total energy using the linearized optimization method. The bulk optimized Jastrow factor was used in both bulk and defective phases to minimize the potential impact of pseudopotential locality errors in the subsequent DMC calculations, similar to what is commonly done for van der Waals systems. In both the bulk and defective cases, the absolute variance to energy ratio resulting from the Jastrow was near 0.026 Ha, indicating uniform quality across the structures. Diffusion Monte Carlo total energies and spin densities were obtained by averaging over a  $2 \times 2 \times 2$  supercell twist grid. DMC runs at each twist were performed with a large population of random walkers ( $\approx 14,000$  walkers per twist) and a small timestep of  $0.005 \text{ Ha}^{-1}$  resulting in an acceptance ratio of 99.6%. Validated [31–33] norm-conserving RRKJ pseudopotentials were used for vanadium (Ne-core) and oxygen (He-core). The T-move scheme was used to maintain the variational principle in DMC calculations involving these non-local pseudopotentials. All QMC related simulation workflows were driven with the Nexus [34] workflow automation system.

Optical gaps were calculated for  $M_1$  VO<sub>2</sub> cells (structure shown in Fig. 5 (a)) containing a single oxygen vacancy in the following manner. A single oxygen vacancy was introduced into a 48 atom VO<sub>2</sub> cell in  $M_1$  phase at each of two inequivalent sites – O(I) and O(II). The atomic structures were then relaxed via DFT using the SCAN functional. A  $4 \times 4 \times 4$  set of supercell twist angles was considered for the search space for minimum band gap. At each twist the direct gap from LDA+U was used as a proxy to select twist angles with greatest likelihood of having a minimum gap. Twist angles with minimum LDA+U direct gap in either spin channels were considered for subsequent DMC optical gap calculations. A selection was made both among twist angles that preserved supercell charge neutrality as well among those that admitted a net supercell charge. This was done for both inequivalent oxygen vacancy sites, resulting in two candidate supercell twist angles for each of the two vacancy structures. The direct gap within each cell consistent with the twisted boundary conditions was then calculated within DMC for each spin channel, by promoting one electron from the highest occupied state to the lowest unoccupied one according to the LDA+U Kohn-Sham eigenvalues, as is standardly done. Gaps obtained in this way represent upper bounds to the minimum possible gap that would result from an exhaustive search over all supercell twists.

Since the oxygen dimer formation energy has different amounts of error in the different methods used, we calculate the oxygen vacancy formation energy in VO<sub>2</sub> using atomic oxygen and bulk VO<sub>2</sub> as reference using this formula:

$$E_f[V_O] = E_{\text{total}}[n(\text{VO}_{2-\delta})] - E_{\text{total}}[n(\text{VO}_2)] - E[\text{O}] \quad (2)$$

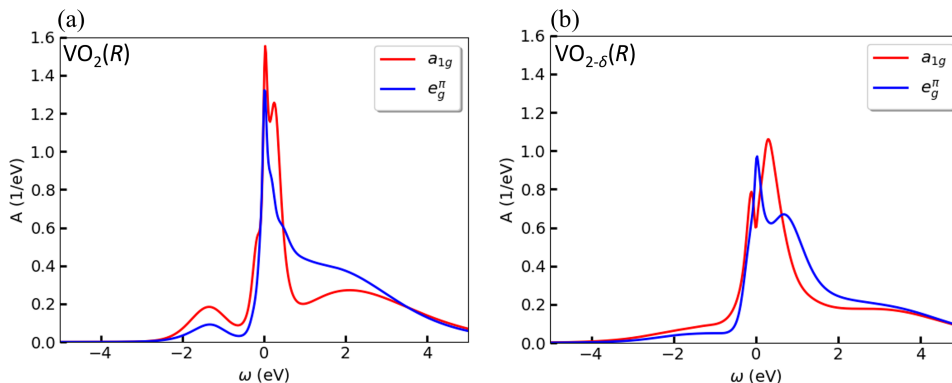


FIG. 3. (a) and (b) show the orbitaly-resolved local  $V-t_{2g}$  spectral functions  $A(\omega)$  obtained from real-space DFT+DMFT supercell calculations for pristine ( $\text{VO}_2$ ) and non-stoichiometric ( $\text{VO}_{2-\delta}$ )  $R$ -phase, respectively. In the pristine case, a lower Hubbard peak at  $\sim 1.35$  eV is seen that is predominantly of  $a_{1g}$  type, indicative of strong electronic correlations. Introducing  $V_O$ 's suppresses both the quasiparticle peak at low energy as well as the Hubbard peak.

where the total energies are calculated at 0K and  $n = 16$  is the number of formula units in our 48-atom supercell, and  $\delta = 0.0625$ .  $E[O]$  is taken to be one-half the total energy of an oxygen dimer.

### c. Dynamical Mean Field Theory (DMFT)

Calculations beyond DFT are put into practice to account for strong electron correlations on the V sites. We use a charge self-consistent DFT+dynamical mean-field theory (DMFT) framework [35], building up on a mixed-basis pseudopotential approach for the DFT part and the continuous-time quantum-Monte-Carlo method, as implemented in the TRIQS package [36, 37], for the DMFT impurity problem. The GGA in the PBE-functional form is employed within the Kohn-Sham cycle. Vanadium 3d4s4p and Oxygen 2s2p were treated as valence electrons in the pseudopotential generation scheme. Locally, threefold effective  $V(3d)$  Wannier-like functions define the correlated subspace, which as a whole consists of the corresponding sum over the various V sites in the defect problem. Projected-local orbitals [38] of 3d character provide the effective functions from acting on Kohn-Sham conduction states above the  $O(2p)$ -dominated band manifold. The selected threefold functions are given by the local three-orbital sector lowest in energy, respectively. Each V site marks an impurity problem, and the number of symmetry-inequivalent vanadium sites provides the number of single-site DMFT problems to solve. A three-orbital Hubbard Hamiltonian of Slater-Kanamori form, parametrized by the Hubbard  $U = 4$  eV and the Hund's exchange  $J_H = 0.7$  eV, acts on each V site. These values for the local Coulomb interactions are close to an effective  $U_{eff} = U - J = 3.5$  eV, which was shown to be optimal in previous studies on  $\text{VO}_2$ . [6, 31] A double-counting correction of the fully-localized form [39] is utilized. The

analytical continuation of the finite-temperature Greens functions on the Matsubara axis  $i\omega$  to real frequencies is performed via the maximum-entropy method as well as with the Padé scheme.

Atomic structures were relaxed using atomic forces obtained from Density Functional Theory (DFT) based calculations with the SCAN functional [25, 26]. All calculations were performed in a 48-atom supercell as shown in Fig. 1(a). Oxygen vacancy structures were obtained by removing one oxygen atom from the 48-atom supercell (i.e. 1 missing oxygen in a 16 f.u.  $\text{VO}_2$  supercell corresponding to  $\text{VO}_{2-\delta}$  with  $\delta=1/16=0.0625$ ). Relaxed structure (shown in Fig.1(b)) suggests a significant degree of local distortion around the  $V_O$  site. It is not immediately clear how important are these distortions in describing the observed suppression of MIT. To assess this, we also perform calculations using a virtual crystal approximation (VCA) method whereby electrons are added to  $\text{VO}_2$  to mimic electronic-doping, without any atomic relaxation/distortion. VCA is site/chemical selective. In more detail, an oxygen-like pseudo-atom of charge  $Z = 8 + \delta$ , i.e. a nominal mixture of an O and an F atom, is utilized within VCA to mimic the appearance of oxygen vacancies. Calculations beyond DFT, such as a charge self-consistent DFT+DMFT method [35–37] employed in a real-space formulation to treat several-coupled impurity problems as well as the Diffusion Monte Carlo (DMC) flavor of continuum QMC method using QMCPACK[6, 30, 31] are put into practise to account for strong electronic correlations on the V sites. Oxygen vacancy formation energy was calculated using Eq. 2.

## III. RESULTS AND DISCUSSION

The  $V_O$  formation energies obtained from DMFT and QMC-calculations are 5.09 and 5.10(1) eV, respectively,

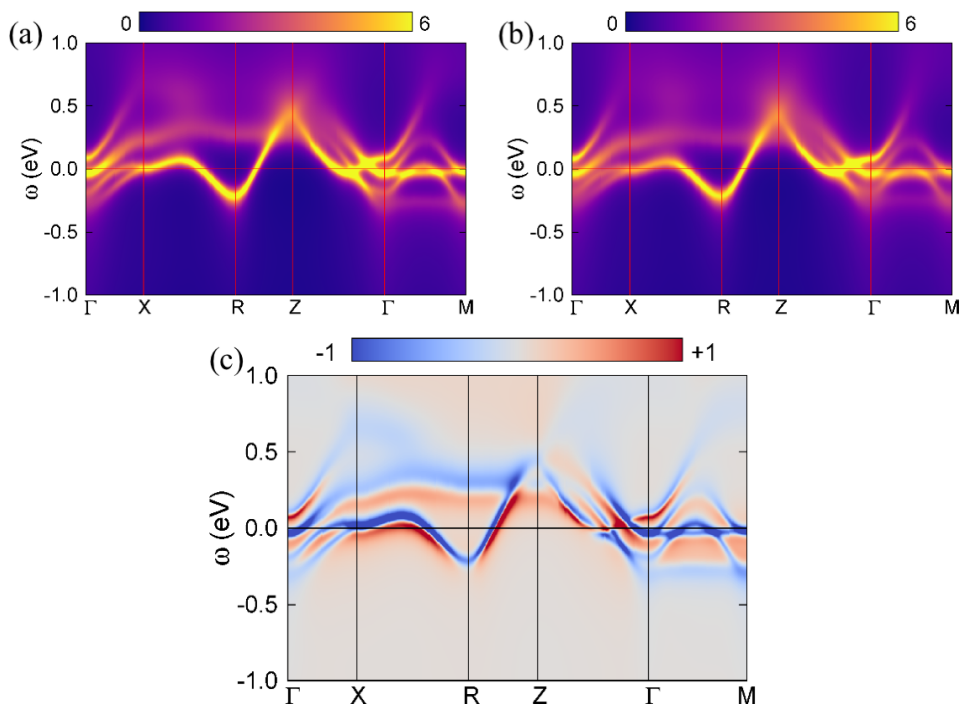


FIG. 4. (a) and (b) show the  $\mathbf{k}$ -resolved spectral function of pristine  $\text{VO}_2$  and  $\text{VO}_{2-\delta}$  (within VCA) for  $\delta \sim 0.06 e^-$ , respectively from our DMFT calculations at  $T \sim 370\text{K}$ . (c) shows the difference of the  $\mathbf{k}$ -resolved spectral function between defective and pristine  $\text{VO}_2$  within VCA, for a charge-doping of  $0.06 e^-$ . Significant reorganization of spectral weights is observed, with a stronger reduction around  $\omega = 0$ .

in excellent agreement with each other. As such both of these strongly-correlated techniques must capture the changes in the underlying electronic structure due to  $V_O$ 's appreciably well, in turn implying a coupling of  $V_O$ 's to the strength of electron correlations. The charge density difference compared to stoichiometric  $\text{VO}_2$  from DMFT and DMC results are shown in Fig. 2 (a) and (b), respectively. While absolute values are not identical, possibly due to different types of pseudopotentials (see Methods), at both levels of theory, the largest change in charge density appears to be around the three vanadium atoms closest to the  $V_O$  as shown in Fig. 1(b). Specifically, QMC charge densities show that the three underbonded  $V_{1,2,3}$  atoms have an excess of electrons compared to pristine  $\text{VO}_2$  (a cutoff distance of  $1.26 \text{ \AA}$  was used for charge integration). A local perturbation of the charge density in the presence of  $V_O$ , as opposed to complete delocalization of the excess electrons from  $V_O$  as one might expect in a regular metal, could be reminiscent of its bad-metal behavior. Also, the agreement between DMFT and DMC on ground-state properties such as vacancy formation energy and charge-density gives greater confidence in the DMFT excited-state properties, such as the spectral function.

Fig. 3(a) shows the orbitally-resolved local spectral function  $A(\omega)$  of  $V-3d^1$  for stoichiometric  $R$ -phase  $\text{VO}_2$  obtained at a temperature of  $T = 370 \text{ K}$ , well

above  $T_{MIT} = 340 \text{ K}$ . In addition to a narrow quasi-particle peak close to  $\omega = 0$ , a lower Hubbard peak is seen at  $\sim 1.35 \text{ eV}$  below the Fermi-level. This is in contrast to the density-of-states obtained from DFT-based methods (see Appendix), but in good agreement with the photoelectron spectroscopy (PES) results [12] that show a small low-energy bump in the valence spectrum of  $\text{VO}_2$  around  $\sim 1 \text{ eV}$ . We find these states to be dominated by  $a_{1g}$  orbital contributions compared to the two degenerate  $e_g^\pi$  orbitals (only the average  $e_g^\pi$  contribution is shown). The same PES experiment [12] shows these localized  $V-3d^1$  states to be occupied even in the insulating  $M$ -phase, but they are now part of the doubly-occupied  $V-V$  dimerized singlet state, which is also composed of the  $a_{1g}$  orbitals. Therefore one might expect that disrupting this near orbital polarization of  $a_{1g}$  orbitals should have an influence on the MIT in  $\text{VO}_2$ . Indeed, X-ray dichroism experiments [17] showed that lowering orbital polarization of  $a_{1g}$  via strain led to a reduced  $T_{MIT}$ . We now explore the influence of  $V_O$ 's on orbital occupancies and the resultant orbital dichroism, defined as  $D_{orb} = (n_{a_{1g}} - n_{e_g^\pi}) / (n_{a_{1g}} + n_{e_g^\pi})$ , where  $n_\alpha$  is the electron-density from the orbital  $\alpha$ , which loosely corresponds to the measured quantity in X-ray dichroism experiments [15, 17].

The orbitally-resolved spectral function from DMFT for  $\text{VO}_{2-\delta}$  [Fig. 3(b)] is very different from that of  $\text{VO}_2$ .

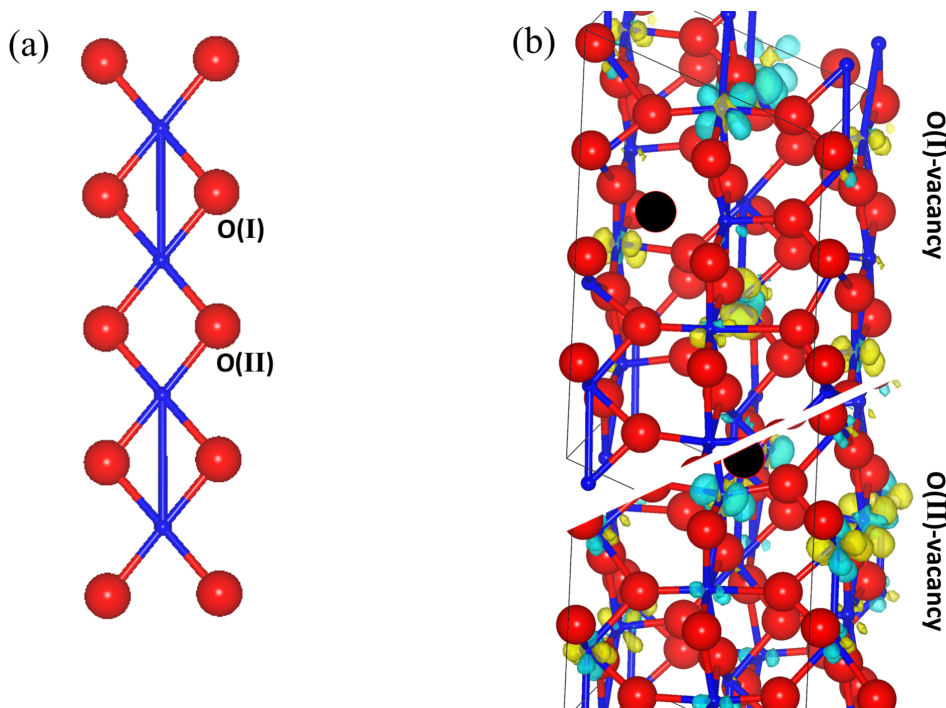


FIG. 5. (a) Fragment of the atomic structure of the  $M_1$  phase of  $\text{VO}_2$  showing the 1D V-V dimerized chain, and the two inequivalent oxygen sites. (b) Shows the charge-density differences corresponding to the lowest optical excitation for the two oxygen vacancies in the  $M_1$  phase. (O(red-sphere), V(blue-sphere),  $\text{O}_v$ (black-sphere), V-V dimer (blue-bonds), isosurface value= $1.1\text{E-}4e^-/\text{\AA}^3$  with +/-= $\text{yellow/green}$ .)

Clearly, the low-energy bump at  $\sim 1.35$  eV has a much-reduced intensity, and the width of the quasiparticle peak has significantly widened, leading to its reduced peak height – suggesting weakened electron-electron correlations. In particular, the  $e_g^\pi$  orbital occupancy appears to be competing with the  $a_{1g}$  occupancy, indicating that the near orbital  $a_{1g}$  polarization seen in  $\text{VO}_2$  is now reduced. The integrated V- $d$  charge is now  $1.12e^-$ , much different from the nominal  $1e^-$  in stoichiometric  $\text{VO}_2$ , and consistent with the QMC charge density analysis discussed above. This strongly indicates that in the presence of  $\text{V}_\text{O}$ , reduction of the near orbital polarization of the  $a_{1g}$  orbital and concomitant weakening of electronic correlations lead to suppression of the MIT.

In order to investigate the importance of capturing the large local distortion seen in our DFT-relaxed structure [Fig. 1(b)] we performed DMFT calculations in the  $\text{VO}_2$  unit-cell using a virtual-crystal approximation (VCA). This results in a 1.12 electron filling of the V site in the converged DFT+DMFT-calculation. The difference plot of the quasiparticle dispersion as shown in Fig. 4(c) is consistent with this electron doping. In addition, loss of k-resolved spectral-weight intensity at low energy is in line with the larger overall quasiparticle weight in the defective case. This suggests that while details of the distortion are necessarily important in getting the correct vacancy-formation energetics as well as

correlating local bond-disproportionation around the defect to charge-reorganization to obtain the correct orbital weights, qualitative changes in the relative orbital occupancies with doping should be captured even in the absence of such localized distortions.

Optical gaps were calculated for  $M_1$   $\text{VO}_2$  cells containing a single oxygen vacancy using DMC (details in Methods section). At each twist the direct gap from LDA+U was used as a proxy to select twist angles with greatest likelihood of having a minimum gap. QMC estimations of the optical band-gap in a 48-atom supercell of the insulating  $M_1$  phase showed a reduction in the gap from 0.8(1) eV in bulk [21] to 0.48(6) or 0.00(6) eV depending on which oxygen-site the vacancy was created. Closing of the gap in the  $M_1$  phase even with the presence of a single vacancy suggests that the insulating state is at the verge of an electronic instability. Charge-density differences corresponding to the lowest optical excitations for the two oxygen vacancy positions in the  $M_1$  phase, as shown in Fig. 5(b), suggest that they are  $d-d$ -type excitations, specifically between  $d$  orbitals in-plane ( $a_{1g}$ ) and out-of-plane ( $e_g^\pi$ 's) containing V-V dimers. Persistence of such gapless  $d-d$ -type excitations therefore indicates absence of the near orbital polarization of  $a_{1g}$  orbitals, consistent with the earlier DMFT results. Suppression of the MIT in non-stoichiometric  $\text{VO}_2$  is consistent with recent experiments where the metallic  $R$ -phase was seen

to be stable even down to 50 K [19]. Since this behavior is experimentally similar to  $W$ -doped  $\text{VO}_2$ , it appears that introducing  $V_O$  in  $\text{VO}_2$  is similar to electronically doping it, even in the metallic phase, as confirmed by DMFT. Given that the changes are local, as inferred from our charge-density plots (Fig. 2), our calculations suggest that there is some kind of a percolation threshold that needs to be exceeded in order to suppress the MIT. This hypothesis is in agreement with experimental observations [19] which estimate a critical doping concentration of  $\delta_c^{exp} = 0.098$  to be necessary to fully suppress the metal-insulator transition.

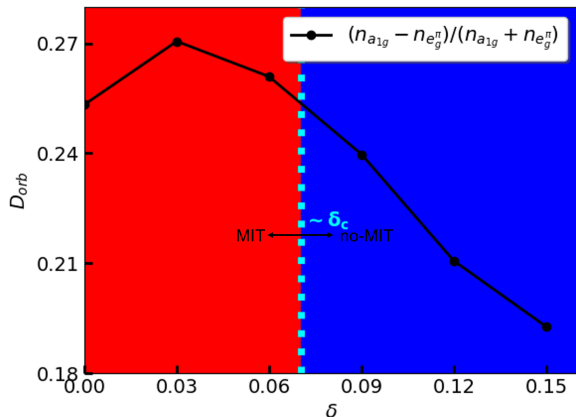


FIG. 6. (a) Orbital-dichroism ( $D_{orb}$ ) from DMFT-VCA calculations shows that with electron-doping the dichroism initially increases, but subsequently becomes less positive with a diminished magnitude. At  $\delta_c \sim 0.07$  its value dips below that of pristine  $\text{VO}_2$ , and is indicative of a doping-level beyond which MIT would be suppressed. This value is close to the experimental estimation of  $\delta_c^{exp}=0.098$  in  $\text{VO}_2$  thin-films.

To see the presence of such a critical concentration, and its relationship as well as manifestation in terms of the suppression of the near orbital-polarization, we estimate  $D_{orb}$  as defined above from VCA calculations performed at a series of doping concentrations ( $\delta$ ) as shown in Fig. 6.  $D_{orb}$  becomes initially more positive with  $\delta$ , but quickly reduces in magnitude, consistent with the expected relative loss of the  $a_{1g}$  orbital-weights. Above  $\delta = \delta_c \sim 0.07$ ,  $D_{orb}$  falls below its pristine  $\text{VO}_2$  value, indicative of a critical concentration above which no MIT can be realized. This observation proves the direct link between suppression of near-orbital polarization of  $a_{1g}$  and the suppression of the MIT. Given that  $D_{orb}$  can be loosely connected to the experimentally measured X-ray dichroism [17], our results suggest that the physics underlying MIT suppression and the tuning of  $T_{MIT}$  in  $\text{VO}_2$  by means of  $V_O$ 's, extrinsic-dopants, strain, or electric fields is very similar, and all of these approaches are different controls to modify the  $a_{1g}$ 's relative occupancy and reduce electron-electron correlations to influence the MIT. X-ray dichroism studies in well-controlled non-stoichiometric  $\text{VO}_2$  thin-films should experimentally

confirm this claim.

Electron-electron correlations are thought to be important for describing the bad-metal behavior of  $\text{VO}_2$  as well as causing V-V dimerization in the  $M$  phase. [14, 15] A 1-D Peierls instability could be driven by a 1-D charge-density wave (CDW) instability, which would correspond to a nesting vector at  $k \sim 2k_F$ , where  $k_F$  is the Fermi wave-vector. If this is indeed the case, it will show up as a ‘bump’ in the momentum distribution  $n(k)$ . When using a value of ‘U’ optimized by DMC, the  $n(k)$  from LSDA+U and DMC have negligible differences for  $k > k_F$  [40], as such we study  $n(k)$  using LSDA+U. Indeed, the  $n(k)$  obtained from our LSDA+U calculation for the  $R$ -phase  $\text{VO}_2$  shows such a bump at  $\sim 2k_F = 2.49$  a.u., where the  $k$  vector is plotted conjugate to the  $\mathbf{c}$  direction as shown in Fig. 7 and recently published by some of us in Ref. [40] No such oscillatory features are observed along the other  $k$ -directions. This shows the presence of a 1-D CDW instability with a nesting vector of  $2k_F$ , which would be required to drive the V-V dimerization, resulting in the insulating  $M$ -phase. The bump is also expected to cause divergences in the response-functions, such as the Lindhard-susceptibility, and thereby lead to its bad-metal behavior – i.e. the violation of the Wiedemann-Franz law [10].

In the presence of  $V_O$ , this bump at  $\sim 2k_F$  vanishes (Fig. 7), altering the bad-metal characteristics of  $\text{VO}_2$ , and the density monotonically decreases with increasing momentum. This would result in divergence-less response functions, and thereby a lack of an electronic instability to drive a phase-transition. This is a consequence of the weakening of electron-electron correlation, as also suggested from our DMFT results, whereby the

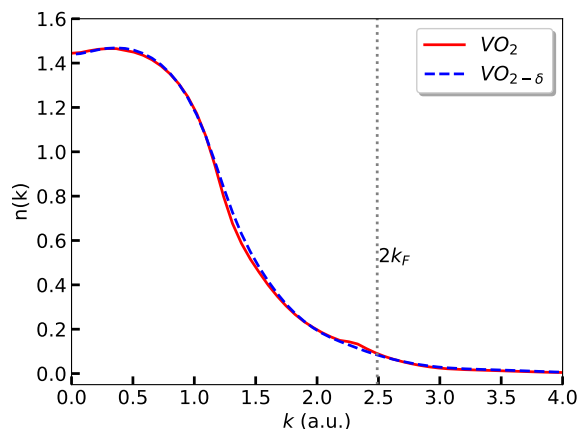


FIG. 7. Momentum density along  $k$  direction conjugate to the V-V dimerization direction for pristine and non-stoichiometric  $\text{VO}_2$  from LSDA+U calculations. Vanishing of the  $\sim 2k_F$  peak in  $\text{VO}_{2-\delta}$  suggests a lack of a charge-density wave (CDW) when  $V_O$ 's are introduced, thereby altering its bad-metal behavior.

filling is not  $1e^-$  on each V site and the near orbital polarization of  $a_{1g}$  is lacking. Suppressing this electronic driving force for a Peierls distortion should also result in suppression of the structural transition to the  $M$ -phase.

#### IV. CONCLUSION

Oxygen-vacancies donate electrons, and the resulting orbital-dependent charge-doping reduces the near orbital polarization of the  $a_{1g}$  orbitals seen in R-phase  $\text{VO}_2$ . This reduction is associated with a weakening of the electronic correlations and leads to a reduced drive for V-V dimerization. This not only suppresses the MIT, but also substantially alters the “bad metal” characteristics of the metallic phase in non-stoichiometric  $\text{VO}_2$ . Our study re-affirms the intricate connection between structural dimerization and electron-correlation in  $\text{VO}_2$ , and suggests that the MIT is predominantly driven by a correlation-induced electronic instability and not a structural instability, with the  $a_{1g}$  occupancy being the primary knob to control the MIT via different external perturbations such as  $V_O$ 's, extrinsic dopants, strain, or electric-fields. This understanding of the presence of a single fundamental knob that allows control over complex coupled phase-transitions in correlated solids can be relevant to engineering functional interfaces of correlated oxides and also aid in understanding technologically relevant MIT systems that show concomitant magnetic- and/or structural-transitions, such as manganites [22] and the family of non-stoichiometric  $\text{ABO}_{3-x}$  compounds. [23]

*Acknowledgement:* Work at Oak Ridge National Laboratory and Argonne National Laboratory was supported by the U.S. Department of Energy, Office of Science, Basic Energy Sciences, Materials Sciences and Engineering Division, as part of the Computational Materials Sciences Program and Center for Predictive Simulation of Functional Materials. This research used resources of the Oak Ridge Leadership Computing Facility at the Oak Ridge National Laboratory, which is supported by the Office of Science of the U.S. Department of Energy under Contract No. DE-AC05-00OR22725. This research used resources of the National Energy Research Scientific Computing Center, a DOE Office of Science User Facility supported by the Office of Science of the U.S. Department of Energy under Contract No. DE-AC02-05CH11231. This manuscript has been authored by UT-Battelle, LLC under Contract No. DE-AC05-00OR22725 with the U.S. Department of Energy. The United States Government retains and the publisher, by accepting the article for publication, acknowledges that the United States Government retains a nonexclusive, paid-up, irrevocable, worldwide license to publish or reproduce the published form of this manuscript, or allow others to do so, for United States Government purposes. The Department of

Energy will provide public access to these results of federally sponsored research in accordance with the DOE Public Access Plan (<http://energy.gov/downloads/oe-public-access-plan>)

FL acknowledges financial support from the DFG project LE 2446/4-1. DFT+DMFT computations were performed at the JURECA Cluster of the Jülich Supercomputing Centre (JSC) under project number hhh08.

#### APPENDIX

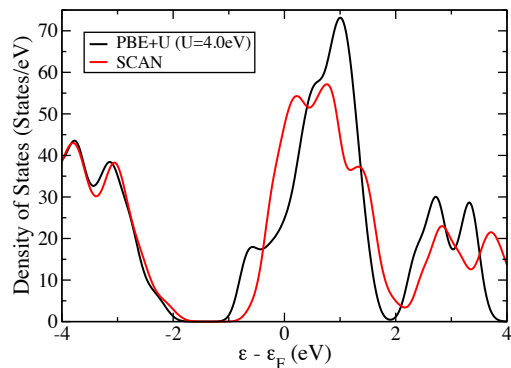


FIG. 8. Total density-of-states for  $\text{VO}_2$  from SCAN and PBE+U calculations.

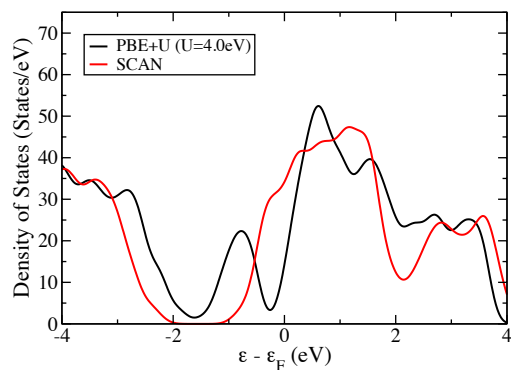


FIG. 9. Total density-of-states for non-stoichiometric  $\text{VO}_2$  from SCAN and PBE+U calculations.

This manuscript has been authored by UT-Battelle, LLC under Contract No. DE-AC05-00OR22725 with the U.S. Department of Energy. The United States Government retains and the publisher, by accepting the article for publication, acknowledges that the United States Government retains a non-exclusive, paid-up,

irrevocable, world-wide license to publish or reproduce the published form of this manuscript, or allow others to do so, for United States Government purposes. The Department of Energy will provide public access to these results of federally sponsored research in accordance with the DOE Public Access Plan (<http://energy.gov/downloads/doe-public-access-plan>).

---

\* ganeshp@ornl.gov

- [1] C. Freysoldt, B. Grabowski, T. Hickel, J. Neugebauer, G. Kresse, A. Janotti, and C. G. Van de Walle, *Rev. Mod. Phys.* **86**, 253 (2014).
- [2] D. B. Strukov, G. S. Snider, D. R. Stewart, and R. S. Williams, *Nature* **453**, 80 (2008).
- [3] J. R. Weber, W. F. Koehl, J. B. Varley, A. Janotti, B. B. Buckley, C. G. Van de Walle, and D. D. Awschalom, *Proceedings of the National Academy of Sciences* **107**, 8513 (2010), <http://www.pnas.org/content/107/19/8513.full.pdf>.
- [4] I. H. Inoue and M. J. Rozenberg, *Advanced Functional Materials* **18**, 2289 (2008).
- [5] N. Shukla, A. V. Thathachary, A. Agrawal, H. Paik, A. Aziz, D. G. Schlom, S. K. Gupta, R. Engel-Herbert, and S. Datta, *Nature Communications* **6**, 7812 (2015).
- [6] Y. Sharma, J. Balachandran, C. Sohn, J. T. Krogel, P. Ganesh, L. Collins, A. V. Ievlev, Q. Li, X. Gao, N. Balke, O. S. Ovchinnikova, S. V. Kalinin, O. Heinonen, and H. N. Lee, *ACS Nano* **12**, 7159 (2018), PMID: 29906092, <https://doi.org/10.1021/acsnano.8b03031>.
- [7] J. Ding, J. Balachandran, X. Sang, W. Guo, J. S. Ansell, G. M. Veith, C. A. Bridges, Y. Cheng, C. M. Rouleau, J. D. Poplawsky, N. Bassiri-Gharb, R. R. Unocic, and P. Ganesh, *Chemistry of Materials* **30**, 4919 (2018), <https://doi.org/10.1021/acs.chemmater.8b00502>.
- [8] A. Zylbersztein and N. F. Mott, *Phys. Rev. B* **11**, 4383 (1975).
- [9] V. J. Emery and S. A. Kivelson, *Phys. Rev. Lett.* **74**, 3253 (1995).
- [10] S. Lee, K. Hippalgaonkar, F. Yang, J. Hong, C. Ko, J. Suh, K. Liu, K. Wang, J. J. Urban, X. Zhang, C. Dames, S. A. Hartnoll, O. Delaire, and J. Wu, *Science* **355**, 371 (2017), <http://science.sciencemag.org/content/355/6323/371.full.pdf>.
- [11] J. B. Goodenough, *Journal of Solid State Chemistry* **3**, 490 (1971).
- [12] C. Blaauw, F. Leenhouts, F. van der Woude, and G. A. Sawatzky, *Journal of Physics C: Solid State Physics* **8**, 459 (1975).
- [13] S. Biermann, A. Poteryaev, A. I. Lichtenstein, and A. Georges, *Phys. Rev. Lett.* **94**, 026404 (2005).
- [14] W. H. Brito, M. C. O. Aguiar, K. Haule, and G. Kotliar, *Phys. Rev. Lett.* **117**, 056402 (2016).
- [15] A. X. Gray, J. Jeong, N. P. Aetukuri, P. Granitzka, Z. Chen, R. Kukreja, D. Higley, T. Chase, A. H. Reid, H. Ohldag, M. A. Marcus, A. Scholl, A. T. Young, A. Doran, C. A. Jenkins, P. Shafer, E. Arenholz, M. G. Samant, S. S. P. Parkin, and H. A. Dürr, *Phys. Rev. Lett.* **116**, 116403 (2016).
- [16] J. D. Budai, J. Hong, M. E. Manley, E. D. Specht, C. W. Li, J. Z. Tischler, D. L. Abernathy, A. H. Said, B. M. Leu, L. A. Boatner, R. J. McQueeney, and O. Delaire, *Nature* **515** (2014).
- [17] N. B. Aetukuri, A. X. Gray, M. Drouard, M. Cossale, L. Gao, A. H. Reid, R. Kukreja, H. Ohldag, C. A. Jenkins, E. Arenholz, K. P. Roche, H. A. Drr, M. G. Samant, and S. S. P. Parkin, *Nature Physics* **9**, 661 (2013).
- [18] N. F. Quackenbush, H. Paik, M. E. Holtz, M. J. Wahila, J. A. Moyer, S. Barthel, T. O. Wehling, D. A. Arena, J. C. Woicik, D. A. Muller, D. G. Schlom, and L. F. J. Piper, *Phys. Rev. B* **96**, 081103 (2017).
- [19] Z. Zhang, F. Zuo, C. Wan, A. Dutta, J. Kim, J. Rensberg, R. Nawrodt, H. H. Park, T. J. Larrabee, X. Guan, Y. Zhou, S. M. Prokes, C. Ronning, V. M. Shalaev, A. Boltasseva, M. A. Kats, and S. Ramanathan, *Phys. Rev. Applied* **7**, 034008 (2017).
- [20] F. Lechermann, W. Heckel, O. Kristanovski, and S. Müller, *Phys. Rev. B* **95**, 195159 (2017).
- [21] H. Zheng and L. K. Wagner, *Phys. Rev. Lett.* **114**, 176401 (2015).
- [22] I. Loa, P. Adler, A. Grzechnik, K. Syassen, U. Schwarz, M. Hanfland, G. K. Rozenberg, P. Gorodetsky, and M. P. Pasternak, *Phys. Rev. Lett.* **87**, 125501 (2001).
- [23] B. Cui, P. Werner, T. Ma, X. Zhong, Z. Wang, J. M. Taylor, Y. Zhuang, and S. S. P. Parkin, *Nature Communications* **9**, 3055 (2018).
- [24] J. Vučićević, D. Tanasković, M. J. Rozenberg, and V. Dobrosavljević, *Phys. Rev. Lett.* **114**, 246402 (2015).
- [25] J. Sun, A. Ruzsinszky, and J. P. Perdew, *Phys. Rev. Lett.* **115**, 036402 (2015).
- [26] J. Sun, R. C. Remsing, Y. Zhang, Z. Sun, A. Ruzsinszky, H. Peng, Z. Yang, A. Paul, U. Waghmare, X. Wu, M. L. Klein, and J. P. Perdew, *Nature Chemistry* **8**, 831 (2016).
- [27] S. L. Dudarev, G. A. Botton, S. Y. Savrasov, C. J. Humphreys, and A. P. Sutton, *Phys. Rev. B* **57**, 1505 (1998).
- [28] G. Kresse and J. Furthmüller, *Phys. Rev. B* **54**, 11169 (1996).
- [29] G. Kresse and D. Joubert, *Phys. Rev. B* **59**, 1758 (1999).
- [30] J. Kim, A. T. Baczewski, T. D. Beaudet, A. Benali, M. C. Bennett, M. A. Berrill, N. S. Blunt, E. J. L. Borda, M. Casula, D. M. Ceperley, S. Chiesa, B. K. Clark, R. C. C. III, K. T. Delaney, M. Dewing, K. P. Esler, H. Hao, O. Heinonen, P. R. C. Kent, J. T. Krogel, I. Kylänpää, Y. W. Li, M. G. Lopez, Y. Luo, F. D. Malone, R. M. Martin, A. Mathuriya, J. McMinis, C. A. Melton, L. Mitas, M. A. Morales, Eric Neuscamman, W. D. Parker, S. D. P. Flores, N. A. Romero, B. M. Rubenstein, J. A. R. Shea, H. Shin, L. Shulenburger, A. F. Tillack, J. P. Townsend, N. M. Tubman, B. V. D. Goetz, J. E. Vincent, D. C. Yang, Y. Yang, S. Zhang, and L. Zhao, *Journal of Physics: Condensed Matter* **30**, 195901 (2018).
- [31] I. Kylänpää, J. Balachandran, P. Ganesh, O. Heinonen, P. R. C. Kent, and J. T. Krogel, *Phys. Rev. Materials* **1**, 065408 (2017).
- [32] J. T. Krogel, J. A. Santana, and F. A. Reboredo, *Phys. Rev. B* **93**, 075143 (2016).
- [33] A. L. Dzubak, J. T. Krogel, and F. A. Reboredo, *The Journal of Chemical Physics* **147**, 024102 (2017), <http://dx.doi.org/10.1063/1.4991414>.
- [34] J. T. Krogel, *Computer Physics Communications* **198**,

- 154 (2016).
- [35] D. Grieger, C. Piefke, O. E. Peil, and F. Lechermann, *Phys. Rev. B* **86**, 155121 (2012).
- [36] O. Parcollet, M. Ferrero, T. Ayrál, H. Hafermann, I. Krivenko, L. Messio, and P. Seth, *Comput. Phys. Commun.* **196**, 398 (2015).
- [37] P. Seth, I. Krivenko, M. Ferrero, and O. Parcollet, *Comput. Phys. Commun.* **200**, 274 (2016).
- [38] B. Amadon, F. Lechermann, A. Georges, F. Jollet, T. O. Wehling, and A. I. Lichtenstein, *Phys. Rev. B* **77**, 205112 (2008).
- [39] V. I. Anisimov, I. V. Solovyev, M. A. Korotin, M. T. Czyżyk, and G. A. Sawatzky, *Phys. Rev. B* **48**, 16929 (1993).
- [40] I. Kylänpää, Y. Luo, O. Heinonen, P. R. C. Kent, and J. T. Krogel, *Phys. Rev. B* **99**, 075154 (2019).